Catal Lett (2014) 144:578–584
DOI 10.1007/s10562-013-1174-4

Effect of Sulfation on the Selective Catalytic Reduction of NO with NH_3 Over γ-Fe_2O_3

Haili Huang · Yi Lan · Wenpo Shan · Feihong Qi · Shangcao Xiong · Yong Liao · Yuwu Fu · Shijian Yang

Received: 8 September 2013 / Accepted: 23 November 2013 / Published online: 12 December 2013

Abstract Because the site for NH_3 adsorption and the active site for NH_3 oxidization were separated after the sulfation, both the SCR reaction and the catalytic oxidization of NH_3 to NO over γ-Fe_2O_3 were restrained after the sulfation. As a result, the operation temperature window of γ-Fe_2O_3 for the SCR reaction shifted about 100 °C to higher temperature after the sulfation.

Keywords Selective catalytic reduction · γ-Fe_2O_3 · Sulfation · Mechanism · Catalytic oxidization of NH_3 to NO

1 Introduction

Selective catalytic reduction (SCR) with NH_3 is proven to be the most promising technology to control the emission of nitrogen oxides from automobile exhaust gas and industrial combustion of fossil fuels [1]. Although V_2O_5/WO_3–TiO_2 has been employed as a commercial SCR catalyst for several decades [2], it is still not satisfactory due to some drawbacks, such as the relatively narrow temperature window of 300–400 °C, the low N_2 selectivity at high temperatures, the toxicity of vanadium pentoxide to the environment [3], and the soaring price of W resource [4]. Therefore, a more cost-effective, better N_2 selectivity and more environmental-friendly SCR catalyst should be developed.

Recently, it is reported that Fe-based catalysts [5–7], for example Fe/ZSM-5 [8, 9], Fe^{3+} exchanged TiO_2-pillared clay [10], Fe–Ti spinel [11], Fe–Ti–V spinel [12], $Fe_2(SO_4)_3$/TiO_2 [13], and iron titanate [14], show excellent SCR activity and N_2 selectivity at 300–400 °C. γ-Fe_2O_3 is one of the simplest iron oxides, which adopts a cubic close packed cation deficient spinel structure [15]. γ-Fe_2O_3 shows the reduction–reoxidation properties, which is suitable for the use as an oxygen storage component in automobile exhaust catalysts [16]. Recently, it is reported that γ-Fe_2O_3 had excellent SCR activity and N_2 selectivity at 200–350 °C [17]. However, the operation temperature window of γ-Fe_2O_3 for the SCR reaction shifted 100 °C to higher temperature in the presence of SO_2 [17]. Generally, the deactivation of SO_2 on the SCR reaction was attributed to the deposition of NH_4HSO_4 and/or $(NH_4)_2SO_4$ at low temperatures [18]. The decomposition temperature of NH_4HSO_4 and/or $(NH_4)_2SO_4$ was less than 250 °C. Therefore, there could be another mechanism, which caused to the deactivation of SO_2 at 250–300 °C. Meanwhile, the SCR activity of γ-Fe_2O_3 was obviously promoted above 300 °C due to the presence of SO_2. Therefore, the mechanism of SO_2 effect on the SCR reaction over γ-Fe_2O_3 need to be further studied. The presence of SO_2 would cause to the sulfation of catalyst [19–21]. The mechanism of the SCR reaction over γ-Fe_2O_3 may differ from that over sulfated γ-Fe_2O_3. Therefore, the sulfation on the SCR reaction over γ-Fe_2O_3 was investigated in this work, which is helpful to understand the mechanism of SO_2 effect on the SCR reaction [22].

Electronic supplementary material The online version of this article (doi:10.1007/s10562-013-1174-4) contains supplementary material, which is available to authorized users.

H. Huang · Y. Lan · W. Shan · F. Qi · S. Xiong · Y. Liao · Y. Fu · S. Yang (✉)
School of Environmental and Biological Engineering, Nanjing University of Science and Technology, Nanjing 210094, People's Republic of China
e-mail: yangshijiangsq@163.com

2 Experimental

2.1 Catalyst Preparation

Nanosized Fe_3O_4, the precursor of γ-Fe_2O_3, was prepared using a co-precipitation method at room temperature [23]. γ-Fe_2O_3 was obtained after the thermal treatment of Fe_3O_4 under air for 3 h at 400 °C [11]. Sulfated γ-Fe_2O_3 was obtained by pretreating γ-Fe_2O_3 (1.0 g) in a flow of 500 ppm SO_2 and 2 % O_2 (200 mL min^{-1}) at 300 °C for 8 h.

2.2 Catalytic Activity Measurement

The SCR reaction was performed on a fixed-bed quartz tube reactor. The mass of catalyst with 40–60 mesh was 100 mg. The total flow rate was 200 mL min^{-1} (room temperature), and the corresponding gas hourly space velocity (GHSV) was 1.2×10^5 cm^3 g^{-1} h^{-1}. The typical reactant gas composition was as follows: 500 ppm of NH_3, 500 ppm of NO, 2 % of O_2, 500 ppm of SO_2 (when used), 10 % of H_2O (when used), and balance of N_2. The concentrations of SO_2, H_2O, NO, NO_2, NH_3 and N_2O were continually monitored by an FTIR spectrometer (MKS Instruments).

2.3 Catalyst Characterization

BET surface area was determined using a nitrogen adsorption apparatus (Quantachrome, Autosorb-1). XRD patterns were recorded on an X-ray diffractionmeter (Rigaku, D/max-2200/PC) between 20° and 80° at a step of 7° min^{-1} operating at 30 kV and 30 mA using Cu Kα radiation. H_2-TPR was recorded on a chemisorption analyzer (Micromeritics, ChemiSorb 2720 TPx) under a 10 % hydrogen-90 % nitrogen gas flow (50 cm^3 min^{-1}) at a rate of 10 °C min^{-1}. Temperature programmed desorption of ammonia (NH_3-TPD) and temperature programmed desorption of NO (NO-TPD) were carried out on the packed-bed microreactor at a rate of 10 °C min^{-1} from 50 to 600 °C. The binding energies of Fe 2p, S 2p and O 1s were recorded on an X-ray photoelectron spectroscopy (Thermo, ESCALAB 250) with Al Kα ($hv = 1486.6$ eV) as the excitation source and C 1s line at 284.6 eV as the reference for the binding energy calibration. In situ DRIFT spectra were performed on a Fourier transform infrared spectrometer (FTIR, Nicolet NEXUS 870) equipped with a liquid-nitrogen-cooled MCT detector, collecting 100 scans with a resolution of 4 cm^{-1}.

3 Results and Discussion

3.1 SCR Activity

As shown in Fig. 1a, γ-Fe_2O_3 showed an excellent SCR activity at 200–350 °C (NO_x conversion was higher than 80 %). During the SCR reaction over γ-Fe_2O_3, only a small amount of N_2O formed above 300 °C. However, NO_x conversion obviously decreased with the increase of reaction temperature from 300 to 400 °C, and a small amount of NO_2 was observed at 350–400 °C. However, NH_3 conversion reached 100 % above 300 °C. It suggests that some NH_3 was oxidized to NO over γ-Fe_2O_3 at 300–400 °C. As 500 ppm of SO_2 was introduced, the SCR activity of γ-Fe_2O_3 obviously decreased at 150–300 °C. However, the SCR activity of γ-Fe_2O_3 was obviously promoted due to the presence of SO_2 at 350–400 °C (shown in Fig. 2). After the further introduction of H_2O, no obvious change happened (shown in Fig. 2). The similar result of γ-Fe_2O_3 was once reported by Mou et al. [17]. As shown in Fig. 2, the SCR activity of γ-Fe_2O_3 in the presence of SO_2 was close to that of sulfated γ-Fe_2O_3 at 300–400 °C. It suggests that the sulfation of γ-Fe_2O_3 could contribute to the effect of SO_2 on the SCR reaction over γ-Fe_2O_3. Therefore, the sulfation on the SCR reaction over γ-Fe_2O_3 was studied.

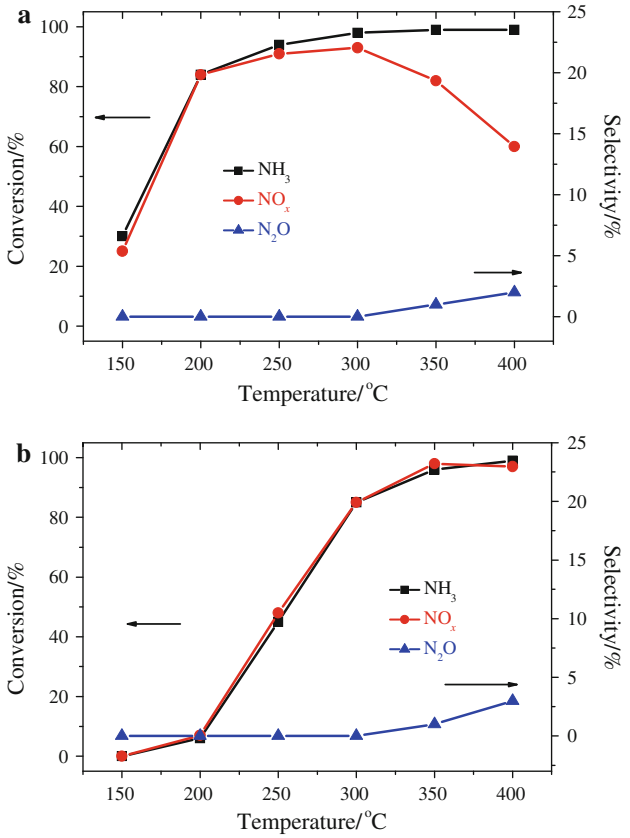

Fig. 1 SCR reaction over:**a** γ-Fe_2O_3, **b** sulfated γ-Fe_2O_3

With the increase of reaction temperature from 150 to 400 °C, NO_x conversion over sulfated γ-Fe_2O_3 gradually increased (shown in Fig. 1b). Figure 1b also shows that the ratio of NO_x conversion was close to that of NH_3 conversion. It suggests that most NH_3 was used to reduce NO over

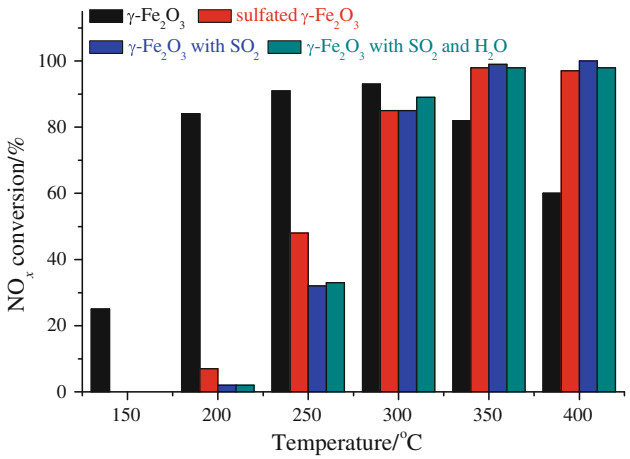

Fig. 2 Effect of SO_2 and/or H_2O on the SCR reaction over γ-Fe_2O_3

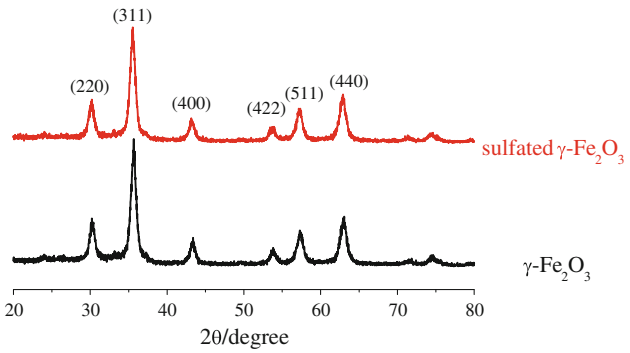

Fig. 3 XRD patterns of γ-Fe_2O_3 and sulfated γ-Fe_2O_3

sulfated γ-Fe_2O_3. Meanwhile, little NO_2 can be observed during the SCR reaction over sulfated γ-Fe_2O_3. In comparison with γ-Fe_2O_3, NO_x conversion over sulfated γ-Fe_2O_3 was much less at 150–300 °C. However, sulfated γ-Fe_2O_3 showed excellent SCR activity (NO_x conversion was higher than 80 %) and N_2 selectivity (>95 %) above 300 °C, which was much better than γ-Fe_2O_3. Figure 1 shows that the operation temperature window of γ-Fe_2O_3 for the SCR reaction shifted about 100 °C to higher temperature after the sulfation.

3.2 Characterization

3.2.1 XRD and BET

As shown in Fig. 3, the characteristic peaks of γ-Fe_2O_3 and sulfated γ-Fe_2O_3 correspond very well to the standard card of maghemite (JCPDS: 39-1346) [15]. It indicates that the spinel structure of γ-Fe_2O_3 was not destroyed after the sulfation.

BET surface areas of γ-Fe_2O_3 and sulfated γ-Fe_2O_3 were 74.7 and 64.8 $m^2\ g^{-1}$, respectively. It indicates that the BET surface area of γ-Fe_2O_3 slightly decreased after the sulfation.

3.3 XPS

As shown in Fig. 4a, the binding energies of Fe 2p 2/3 on γ-Fe_2O_3 mainly centered at about 710.2, 711.1 and 712.5 eV, which were assigned to Fe^{3+} in the spinel structure and Fe^{3+} bonded with hydroxyl groups respectively [15]. Furthermore, the satellite component appeared at about 719.0 eV, which is the fingerprint of Fe^{3+} species [23]. They both suggest that Fe species on γ-Fe_2O_3 were mainly Fe^{3+}. The O 1s peaks on γ-Fe_2O_3 mainly centered at about 530.2 eV and 531.6 eV (shown in Fig. 4b), which were attributed to O^{2-} in transition metal oxides and that in –OH respectively [24]. As shown in Fig. 4c, no obvious S 2p band was observed on γ-Fe_2O_3.

As shown in Fig. 4d, a new peak at 713.8 eV appeared in the spectral region of Fe 2p after the sulfation of γ-Fe_2O_3, which could be attributed to Fe^{3+} in $Fe_2(SO_4)_3$ [23]. Meanwhile, XPS analysis shows that the percent of Fe^{3+} on γ-Fe_2O_3 decreased from 40 to 31.3 % after the sulfation. The presence of SO_4^{2-} on sulfated γ-Fe_2O_3 can also be supported by the XPS spectra over S 2p and O 1s regions. A new peak at 532.1 eV appeared in the spectral region of O 1s (shown in Fig. 4e), which could be assigned to O^{2-} in SO_4^{2-} [25]. The S 2p peaks mainly centered at 168.9 and 169.9 eV (shown in Fig. 4f), which could be assigned to SO_4^{2-} and HSO_4^- respectively [15]. Previous research on the heterogeneous uptake of SO_2 on γ-Fe_2O_3 also demonstrated that the formed S species on iron oxides were mainly HSO_4^- and SO_4^{2-} [26]. XPS analysis shows that the percent of S(SO_4^{2-}) on γ-Fe_2O_3 increased to 5.4 % after the sulfation.

3.4 TPR

TPR profile recorded from γ-Fe_2O_3 showed two obvious reduction peaks. The peak centered at about 318 °C was assigned to the reduction of γ-Fe_2O_3 to Fe_3O_4 [27], and the slight fluctuation at about 350 °C may be related to the impurity on γ-Fe_2O_3. The broad peak at higher temperature was attributed to the reduction of Fe_3O_4 to Fe [27].

The active site on γ-Fe_2O_3 for H_2 oxidization was covered by SO_4^{2-} after the sulfation. Hence, a strong displacement of the first reduction peak to 423 °C happened in the TPR profiles of sulfated γ-Fe_2O_3 (shown in Fig. 5). It suggests that the oxidization ability of γ-Fe_2O_3 decreased after the sulfation. Meanwhile, no obvious changes happened on the broad peak at higher temperature. The reduction peak at 423 °C of sulfated γ-Fe_2O_3 could be attributed to the reduction of Fe^{3+}–SO_4^{2-}. TPR analysis shows that the area ratio of the first peak to the total TPR

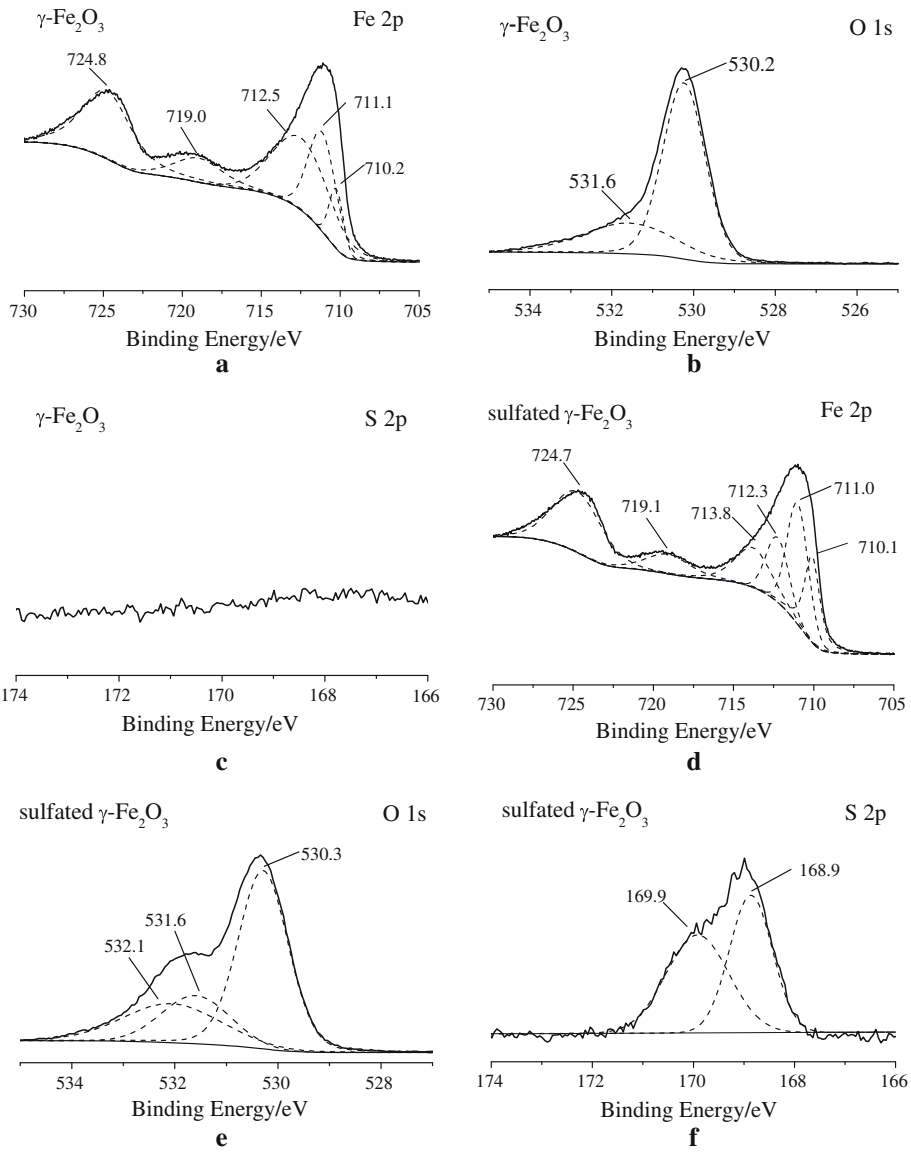

Fig. 4 XPS spectra of γ-Fe_2O_3 and sulfated γ-Fe_2O_3 over the spectral regions of Fe 2p, O 1s and S 2p

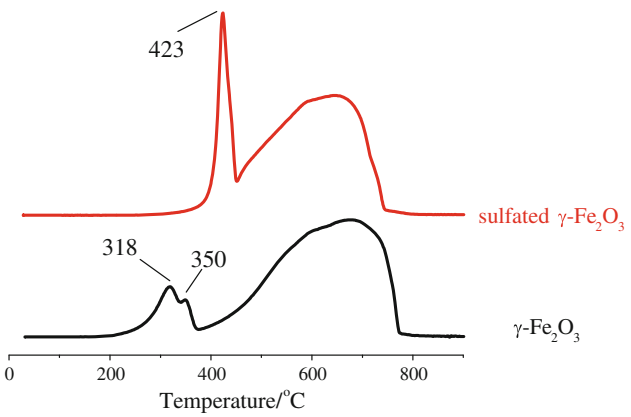

Fig. 5 H_2-TPR profiles of γ-Fe_2O_3 and sulfated γ-Fe_2O_3

profile increased from 13 % for γ-Fe_2O_3 to 19 % for sulfated γ-Fe_2O_3. It also suggests that the reduction of γ-Fe_2O_3 to Fe_3O_4 and the reduction of SO_4^{2-} both contributed to the first reduction peak of sulfated γ-Fe_2O_3.

3.5 NO-TPD and NH_3-TPD

The capacities of γ-Fe_2O_3 and sulfated γ-Fe_2O_3 for NH_3 and NO + O_2 adsorption were calculated from NH_3-TPD and NO-TPD (shown in Fig. S1). The capacity of sulfated γ-Fe_2O_3 for NH_3 adsorption was 5.1 mmol g^{-1}, which was about 4.3 times that of γ-Fe_2O_3 (1.2 mmol g^{-1}). However, the capacity of sulfated γ-Fe_2O_3 for NO + O_2 adsorption was 0.32 mmol g^{-1}, which was only about 1/5 that of γ-Fe_2O_3 (1.7 mmol g^{-1}). It suggests that the adsorption of

NH_3 on γ-Fe_2O_3 was promoted and the adsorption of NO on γ-Fe_2O_3 was restrained after the sulfation.

3.6 Adsorption of NO and NH_3

The characteristic vibration corresponding to the adsorption of NO + O_2 on γ-Fe_2O_3 at 300 °C mainly appeared at about 1,600 and 1,578 cm^{-1} (shown in Fig. 6a), which were assigned to monodentate nitrite and monodentate nitrate respectively [28]. However, the characteristic vibration corresponding to the adsorption of NO + O_2 on sulfated γ-Fe_2O_3 at 300 °C appeared at 1,385 cm^{-1} (shown in Fig. 6a). Monodentate nitrite and monodentate nitrate adsorbed on γ-Fe_2O_3 were coordinated by oxygen atom. However, the oxygen atom on γ-Fe_2O_3, which can be used to bridge NO and Fe cation, was covered by SO_4^{2-} after the sulfation. Therefore, the characteristic vibration at 1,385 cm^{-1} was assigned to nitro [28], which is coordinated via its N atom [19]. The intensity of the adsorption of NO + O_2 on sulfated γ-Fe_2O_3 was much less than that on γ-Fe_2O_3. It indicates that the adsorption of NO_x on γ-Fe_2O_3 was restrained after the sulfation.

The characteristic vibration corresponding to NH_3 adsorption on γ-Fe_2O_3 at 300 °C mainly appeared at about 1,202 and 1,609 cm^{-1} (shown in Fig. 6b), which were assigned to coordinated ammonia bound to the Lewis acid sites [14]. However, the characteristic vibration corresponding to NH_3 adsorption on sulfated γ-Fe_2O_3 appeared at 1,426 and 1,298 cm^{-1} (shown in Fig. 6b), which were assigned to ammonium ions bound to the Brønsted acid sites [22]. The intensity of the adsorption of NH_3 on sulfated γ-Fe_2O_3 was much higher than that on γ-Fe_2O_3. It indicates that the adsorption of NH_3 on γ-Fe_2O_3 was promoted after the sulfation, which was consistent with the result of NH_3-TPD. Meanwhile, a negative peak at about 1,373 cm^{-1} appeared on sulfated γ-Fe_2O_3. XPS analysis demonstrates that γ-Fe_2O_3 was covered by SO_4^{2-} after the sulfation. As is well known, SO_4^{2-} is a typical Brønsted acid [29], so NH_3 mainly adsorbed on SO_4^{2-} on sulfated γ-Fe_2O_3. Therefore, the negative peak at about 1,373 cm^{-1} could be ascribed to SO_4^{2-}, which was covered by NH_4^+ after the adsorption of NH_3 [22].

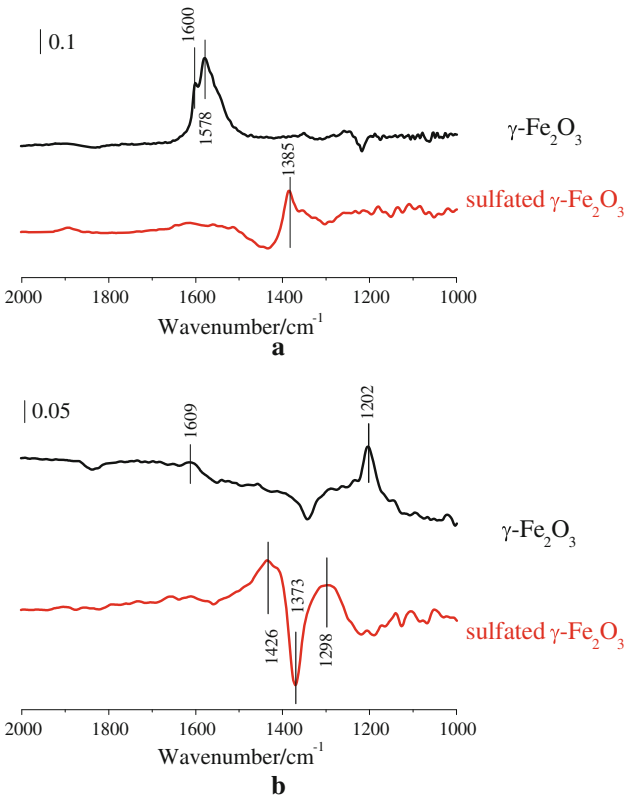

Fig. 6 **a** DRIFT spectra of the adsorption of NO + O_2 on γ-Fe_2O_3 and sulfated γ-Fe_2O_3 at 300 °C, **b** DRIFT spectra of the adsorption of NH_3 on γ-Fe_2O_3 and sulfated γ-Fe_2O_3 at 300 °C

3.7 Mechanism of the Sulfation on the SCR Reaction

Both the Eley–Rideal mechanism (the reaction of activated NH_3 with gaseous NO) and the Langmuir–Hinshelwood mechanism (the reaction between adsorbed NO_x and NH_3) could contribute to the SCR reaction over γ-Fe_2O_3 and sulfated γ-Fe_2O_3. Furthermore, the catalytic oxidization of NH_3 to NO [21] can happen at high temperatures (shown in Table S1).

The SCR reaction and the catalytic oxidization of NH_3 to NO both contributed to NH_3 conversion over γ-Fe_2O_3 and sulfated γ-Fe_2O_3. Therefore, the ratio of NH_3 conversion over γ-Fe_2O_3 and that over sulfated γ-Fe_2O_3 can be described as:

$$NH_3 \text{ conversion } \% = \delta_{SCR} + \delta_{C-O}, \quad (1)$$

where δ_{SCR} and δ_{C-O} were the contributions of the SCR reaction and the catalytic oxidization of NH_3 to NO to the ratio of NH_3 conversion, respectively.

The SCR reaction contributed to the reduction of gaseous NO, while the catalytic oxidization of NH_3 to NO contributed to the formation of gaseous NO. Therefore, the ratio of NO conversion over γ-Fe_2O_3 and that over sulfated γ-Fe_2O_3 can be described as:

$$NO \text{ conversion } \% = \delta_{SCR} - \delta_{C-O} \quad (2)$$

According to Eqs. 1 and 2, the amount of NH_3 conversion assigned to the SCR reaction and that assigned to the catalytic oxidization of NH_3 to NO can be calculated according to the difference between the ratio of NO conversion and that of NH_3 conversion.

Figure 7a shows that the SCR reaction over γ-Fe_2O_3 was obviously promoted with the increase of reaction temperature. However, the catalytic oxidization of NH_3 to NO happened over γ-Fe_2O_3 above 250 °C, resulting in a drop of

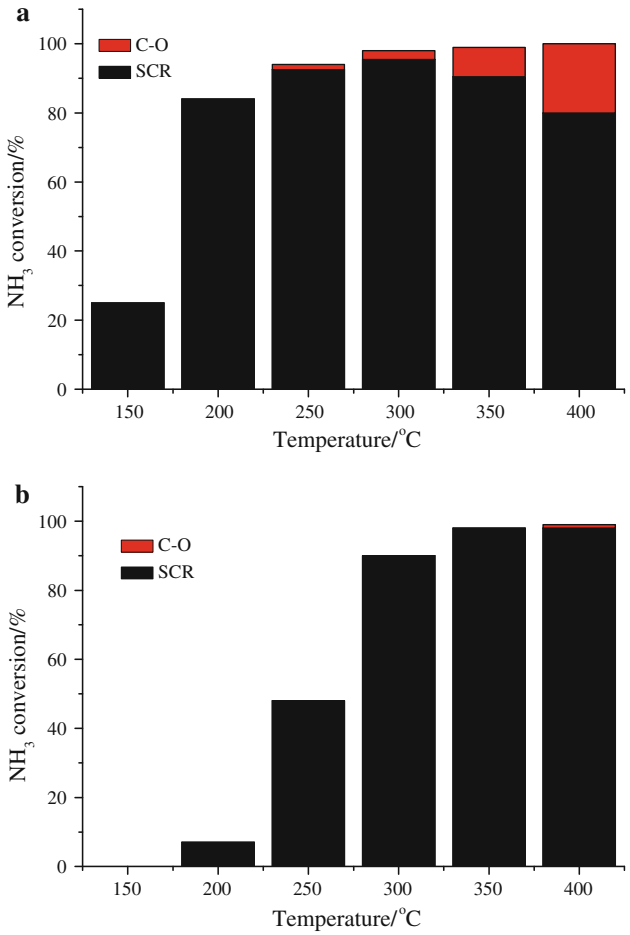

Fig. 7 Contributions of the SCR reaction and the catalytic oxidization of NH_3 to NO (C–O) to NH_3 conversion during the SCR reaction over: **a** γ-Fe_2O_3, **b** sulfated γ-Fe_2O_3

NO_x conversion (shown Fig. 1a). After the sulfation, the SCR reaction over γ-Fe_2O_3 was obviously restrained, resulting in a remarkable decrease of NO conversion at 150–300 °C. Meanwhile, the catalytic oxidization of NH_3 to NO over γ-Fe_2O_3 above 250 °C was suppressed after the sulfation. As a result, the operation temperature window of γ-Fe_2O_3 for the SCR reaction shifted about 100 °C to higher temperature after the sulfation.

The acid sites on γ-Fe_2O_3 (Lewis acid) mainly resulted from the unsaturated coordination between Fe^{3+} and O^{2-}. The unsaturated coordination was destroyed after the sulfation, and the acid sites on sulfated γ-Fe_2O_3 mainly resulted from SO_4^{2-} on the surface. Therefore, NH_3 mainly adsorbed on Fe^{3+} (or Fe–O band) on γ-Fe_2O_3, while it mainly adsorbed on SO_4^{2-} on sulfated γ-Fe_2O_3. It suggests that the site for NH_3 adsorption and the active site for NH_3 activation on γ-Fe_2O_3 were separated after the sulfation (illustrated in Fig. 8). Meanwhile, the oxidization ability of Fe^{3+} on sulfated γ-Fe_2O_3 was less than that on γ-Fe_2O_3, which was hinted by the TPR analysis (shown in Fig. 5). Moreover, the concentration of Fe^{3+} on sulfated γ-Fe_2O_3 was slightly less than that on γ-Fe_2O_3. As a result, the activation of adsorbed NH_3 over γ-Fe_2O_3 was restrained after the sulfation. It suggests that the SCR reaction over γ-Fe_2O_3 through the Eley–Rideal mechanism would be obviously restrained after the sulfation. Furthermore, NO-TPD analysis and in situ DRIFTS study show that the adsorption of NO + O_2 on γ-Fe_2O_3 was restrained after the sulfation. It suggests that the SCR reaction through the Langmuir–Hinshelwood mechanism would be restrained after the sulfation. As a result, the SCR reaction over γ-Fe_2O_3 was restrained after the sulfation (shown in Fig. 7).

Figure 1b shows that most of adsorbed NH_3 on sulfated γ-Fe_2O_3 can be transformed above 300 °C, so the negative effect of sulfation on the SCR reaction over γ-Fe_2O_3 above 300 °C can be neglected. Therefore, the key factor of NO reduction over γ-Fe_2O_3 at high temperatures was the negative effect of the catalytic oxidization of activated NH_3 species (–NH_2) to NO.

–NH_2 mainly adsorbed on Fe^{3+} (or Fe–O band) on γ-Fe_2O_3, while it mainly adsorbed on SO_4^{2-} on sulfated γ-Fe_2O_3. It suggests that the site for –NH_2 adsorption and the active site for the further oxidization of –NH_2 were separated after the sulfation, which was similar to that for NH_3 activation. Meanwhile, the concentration of Fe^{3+} on sulfated γ-Fe_2O_3 was less than that on γ-Fe_2O_3. Moreover, the concentration of –NH_2 on sulfated γ-Fe_2O_3 was much less than that on γ-Fe_2O_3 due to the depression of NH_3

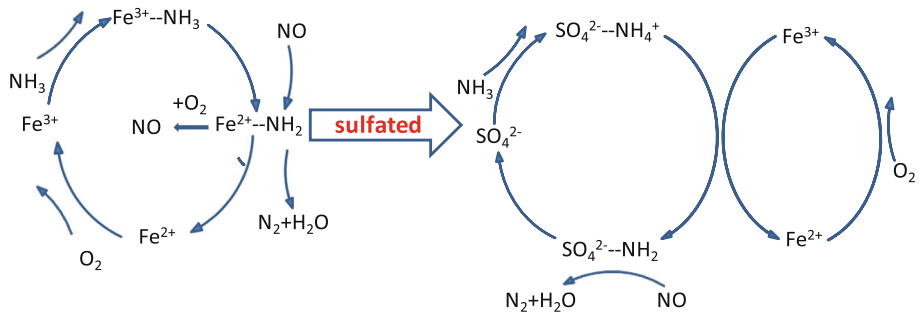

Fig. 8 Illustration of sulfation on the SCR reaction over γ-Fe_2O_3

activation. As a result, the catalytic oxidization of NH_3 to NO over γ-Fe_2O_3 was obviously restrained after the sulfation (shown in Fig. 7).

4 Conclusions

Because the site for NH_3 adsorption and the active site for NH_3 activation were separated, the SCR reaction over γ-Fe_2O_3 was restrained at 150–300 °C after the sulfation. Meanwhile, the catalytic oxidization of NH_3 to NO over γ-Fe_2O_3 was restrained after the sulfation, so the drop of NO_x conversion at high temperatures postponed. As a result, the operation temperature window of γ-Fe_2O_3 for the SCR reaction shifted about 100 °C to higher temperature after the sulfation.

Acknowledgments This study was financially supported by the National Natural Science Fund of China (Grant No. 21207067 and 41372044), the Fundamental Research Funds for the central Universities (Grant No. 30920130111023), the Zijin Intelligent Program, Nanjing University of Science and Technology (Grant No. 2013-0106), Environmental scientific research of Jiangsu Province (2012026), and special fund of State Key Joint Laboratory of Environment Simulation and Pollution Control.

References

1. Topsoe NY (1994) Science 265:1217
2. Chen L, Li JH, Ge MF, Zhu RH (2010) Catal Today 153:77
3. Chen L, Li JH, Ge MF (2010) Environ Sci Technol 44:9590
4. Yang SJ, Wang CZ, Ma L, Peng Y, Qu Z, Yan NQ, Chen JH, Chang HZ, Li JH (2013) Catal Sci Technol 3:161
5. Akah AC, Nkeng G, Garforth AA (2007) Appl Catal B 74:34
6. Chmielarz L, Kustrowski P, Rafalska-Lasocha A, Dziembaj R (2005) Appl Catal B 58:235
7. Yao GH, Gui KT, Wang F (2010) Chem Eng Technol 33:1093
8. Grossale A, Nova I, Tronconi E, Chatterjee D, Weibel M (2008) J Catal 256:312
9. Brandenberger S, Krocher O, Tissler A, Althoff R (2008) Catal Rev 50:492
10. Long RQ, Yang RT (1999) J Catal 186:254
11. Yang SJ, Li JH, Wang CZ, Chen JH, Ma L, Chang HZ, Chen L, Peng Y, Yan NQ (2012) Appl Catal B 117:73
12. Yang S, Wang C, Chen J, Peng Y, Ma L, Chang H, Liu C, Li J, Yan N (2012) Catal Sci Technol 2:915
13. Ma L, Li JH, Ke R, Fu LX (2011) J Phys Chem C 115:7603
14. Liu FD, He H, Zhang CB, Feng ZC, Zheng LR, Xie YN, Hu TD (2010) Appl Catal B 96:408
15. Yang S, Guo Y, Yan N, Wu D, He H, Qu Z, Yang C, Zhou Q, Jia J (2011) ACS Appl Mater Interface 3:209
16. Ayub I, Berry FJ, Crabb E, Helgason O (2004) J Mater Sci 39:6921
17. Mou XL, Zhang BS, Li Y, Yao LD, Wei XJ, Su DS, Shen WJ (2012) Angew Chem Int Edit 51:2989
18. Xie GY, Liu ZY, Zhu ZP, Liu QY, Ge J, Huang ZG (2004) J Catal 224:36
19. Yang SJ, Guo YF, Chang HZ, Ma L, Peng Y, Qu Z, Yan NQ, Wang CZ, Li JH (2013) Appl Catal B 136:19
20. Gu T, Liu Y, Weng X, Wang H, Wu Z (2010) Catal Commun 12:310
21. Yang SJ, Liu CX, Chang HZ, Ma L, Qu Z, Yan NQ, Wang CZ, Li JH (2013) Ind Eng Chem Res 52:5601
22. Liu FD, Asakura K, He H, Shan WP, Shi XY, Zhang CB (2010) Appl Catal B 103:369
23. Yang S, Yan N, Guo Y, Wu D, He H, Qu Z, Li J, Zhou Q, Jia J (2011) Environ Sci Technol 45:1540
24. Yang S, Guo Y, Yan N, Qu Z, Xie J, Yang C, Jia J (2011) J Hazard Mater 186:508
25. Yang S, Guo Y, Yan N, Wu D, He H, Xie J, Qu Z, Jia J (2011) Appl Catal B 101:698
26. Fu HB, Wang X, Wu HB, Yin Y, Chen JM (2007) J Phys Chem C 111:6077
27. Yang S, Wang C, Li J, Yan N, Ma L, Chang H (2011) Appl Catal B 110:71
28. Hadjiivanov KI (2000) Catal Rev 42:71
29. Xie GY, Liu ZY, Zhu ZP, Liu QY, Ge J, Huang ZG (2004) J Catal 224:42